Geophysical Journal International

Geophys. J. Int. (2015) **203,** 2287–2302 doi: 10.1093/gji/ggv428
GJI Marine geosciences and applied geophysics

Tsunami scenarios and hazard assessment along the northern coast of Haiti

A. Gailler,[1] E. Calais,[2] H. Hébert,[1] C. Roy[2] and E. Okal[3]

[1] *CEA, DAM, DIF, F-91297 Arpajon, France. E-mail: audrey.gailler@cea.fr*
[2] *Department of Geosciences, Ecole normale supérieure, PSL Research University, Paris, France*
[3] *Department of Earth & Planetary Sciences, Northwestern University, Evanston, IL 60208, USA*

Accepted 2015 October 1. Received 2015 October 1; in original form 2015 March 30

SUMMARY

The northeastern Caribbean island arc, which materializes the boundary between the North American and Caribbean plates, is particularly exposed to large earthquakes and tsunamis. The low level of preparedness of a large part of its population and the lack of risk reduction provisions in public policies in many countries of the region put their population and economy at high risk in case of large telluric events. Here, we investigate the impact of three possible earthquake scenarios, consistent with the regional seismotectonic setting, on northern Haiti through inundation by tsunami waves. These scenarios simulate the effect of a *M*8.0 earthquake on the Septentrional strike-slip fault (possibly similar to the 1842 earthquake), a *M*8.1 earthquake on the offshore thrust fault system north of Haiti, and an earthquake rupturing a large portion of the offshore thrust fault system north of Haiti and the Dominican Republic. We calculate run-up heights along the northern coast of Haiti, in particular in the densely populated Cap Haitien. We find that the rupture of the offshore North Hispaniola thrust fault could result in wave heights up to 10 m with inundation up to 4 km inland, with only 10–15 min between ground shaking and the first wave arrivals. The city of Cap Haitien is particularly exposed, with potential flooding of most of the city and its suburbs, including the international airport. We also find that the historical reports available for the 1842 earthquake, when compared to our simulations, favor a rupture of the North Hispaniola thrust fault, although much uncertainty remains. If the 1842 earthquake did not rupture the Septentional fault offshore Haiti, then it is currently capable of at least a M_w7.7 earthquake, significantly larger than previously thought. The simulations presented here provide a basis for developing conservative maps of run-up heights that can be transferred, with added factors of safety, into practical implementation for tsunami preparedness and protection.

Key words: Numerical solutions; Tsunamis; Wave propagation; Atlantic Ocean.

1 INTRODUCTION

The northeastern Caribbean region and its population are particularly exposed and vulnerable to earthquakes and tsunamis, as demonstrated by the historical record (e.g. Scherer 1912; O'Loughlin & Lander 2003; McCann 2006; ten Brink *et al.* 2011). The significant population density in coastal areas and their limited level of preparedness are of concern, although progress is being made in the framework of the Caribbean Tsunami Warning System (CTWS, von Hillebrandt-Andrade *et al.* 2013; Saurel *et al.* 2014). Several historical tsunamis have caused significant casualties in the coastal regions of this active plate boundary (Fig. 1) in 1946 (northeastern Dominican republic), 1918 (Mona passage), 1867 (Virgin Islands), 1842 (northern Haiti) and 1692 (Port Royal, Jamaica). These events remain however poorly understood as their relationship with the regional seismogenic sources is not clearly established. More recently, the devastating 2010, M_w7.0 Haiti earthquake (Calais *et al.* 2010) was also accompanied by local tsunami waves that caused at least three fatalities (Fritz *et al.* 2013), a number dwarfed by the 200 000+ deaths caused by structural failures as a direct result of ground shaking. This earthquake served as a tragic reminder of the exposure and vulnerability of most of the region to significant telluric events, earthquakes and tsunamis alike, and called for new efforts to improve our knowledge of the hazard sources and increase the preparedness level in the country and across the region.

In addition to the Port-au-Prince area and more generally the southern part of the country, which lies within short distance of the active Enriquillo fault system (Fig. 1, Mann *et al.* 1995), the northern coast of Haiti is of particular concern because it follows the trace of the near-shore Septentrional strike-slip fault and of the offshore

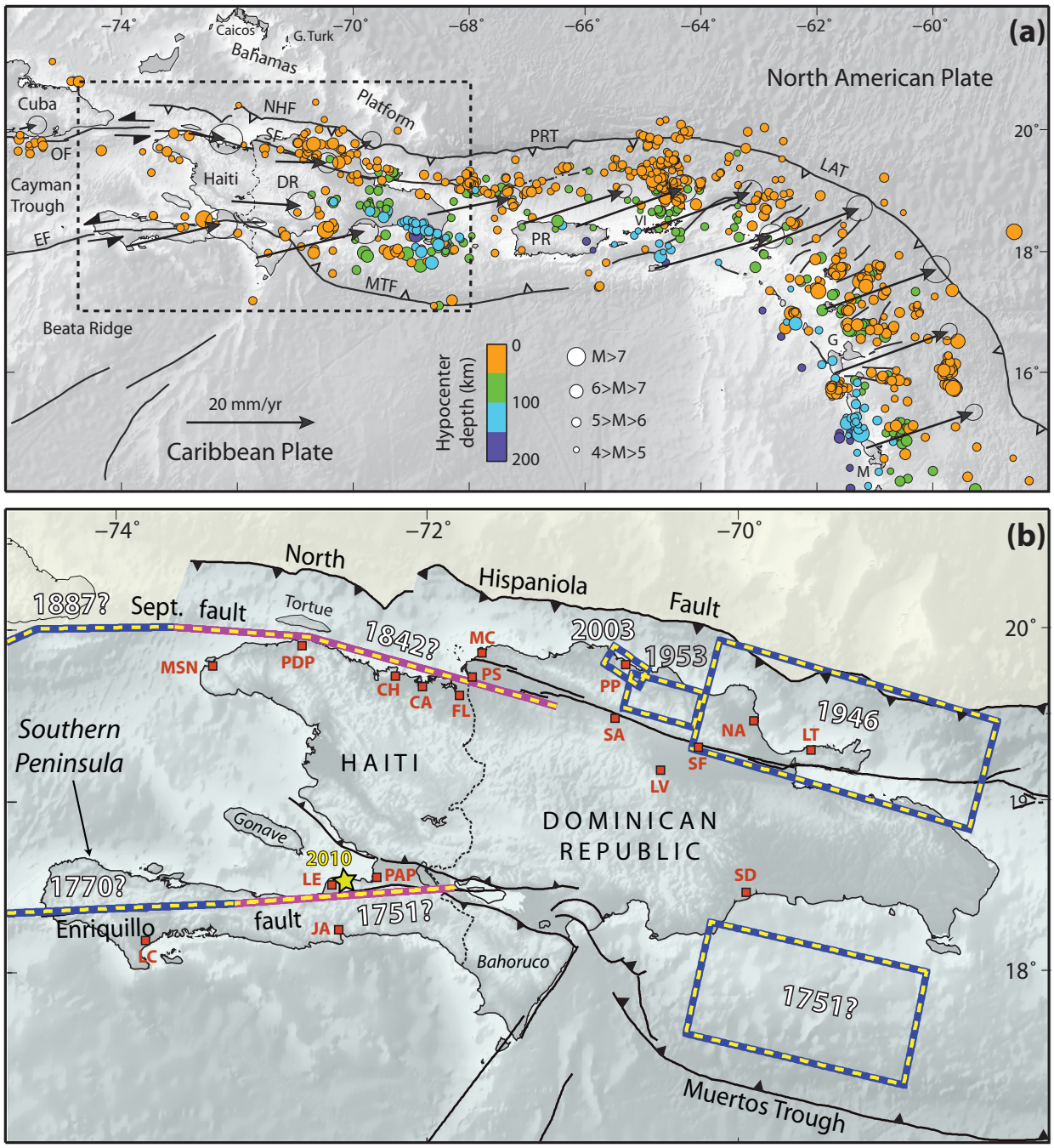

Figure 1. (a) Tectonic setting of the northeastern Caribbean, where the Caribbean and North American plate converge very obliquely at ∼19 mm yr^{-1}. Earthquakes are from the Engdahl *et al.* (1998) catalog. Arrows show GPS velocities at selected sites from Symithe *et al.* (2015). Solid black lines delineate major active faults (OF, Oriental fault; SF, Septentrional fault; NHF, North Hispaniola fault; PRT, Puerto Rico trench; LAT, Lesser Antilles trench; EF, Enriquillo fault; MTF, Muertos trough). DR, Dominican Republic; PR, Puerto Rico; VI, Virgin Islands; G, Guadeloupe; M, Martinique. (b) Close up on Hispaniola showing estimated historical ruptures derived from archives (CITE). Vertical strike-slip events are shown as lines; dip-slip events are shown as projected surface areas. Red squares show the location of some major cities (MSN, Môle St Nicolas; PDP, Port de Paix; CH, Cap Haitien; CA, Caracol; FL, Fort Liberté; PS, Pepillo Salcedo; MC, Monte Cristi; PP, Puerto Plata; SA, Santiago; LV, La Vega; SF, San Francisco de Macoris; NA, Nagua; T, Las Terrenas; SD, Santo Domingo; PAP, Port au Prince; LE, Leogane; JA, Jacmel; LC, Les Cayes). The epicenter of the 2010, M_w7.1 Haiti earthquake is indicated with a yellow star.

North Hispaniola thrust fault (Fig. 1). Both faults are currently accruing elastic strain (Manaker *et al.* 2008) and are the potential sources of significant earthquakes (Frankel *et al.* 2011) that could affect the highly populated cities of Port-de-Paix and Cap Haitien through ground shaking and/or tsunami inundation. This risk indeed materialized on 1842 May 7, when a tsunamigenic earthquake struck the region causing 5000 fatalities in Cap Haitien, half of the population of the coastal city at the time (Scherer 1912). The earthquake was accompanied by a tsunami that caused ∼300 deaths with wave heights of ∼2 m along the northeastern Haitian coast and a maximum run-up of 4.6 m in Port-de-Paix (O'Loughlin & Lander 2003). This event is commonly associated with the

well-known Septentrional strike-slip fault, as indicated on Fig. 1(b) (McCann 2006; Tabrez Ali *et al.* 2008; ten Brink *et al.* 2011). The possibility however exists that it was caused by the North Hispaniola thrust fault further offshore, source of the $M = 8.1$ tsunamigenic earthquake that struck the northeastern Dominican Republic in August 1946 (Fig. 1, Dolan & Wald 1998).

The risk level in northern Haiti prompted international efforts to improve our understanding of the tsunami hazard level in order to set accurate guidelines for preparedness and protection. In this paper, we explore earthquake scenarios for northern Haiti following the recommendation of the 2013 IOC Meeting of Experts (Intergovernmental Oceanographic Commission Workshop Report No. 255): a *M*8.0 earthquake on the Septentrional strike-slip fault (possibly similar to the 1842 May 7 event), a remake of the $M = 8.1$, 1946 August 4 Dominican Republic earthquake but on the offshore thrust fault system north of Haiti, and an earthquake rupturing a large portion of the offshore thrust fault system north of Haiti and the Dominican Republic. The first two scenarios are possible analogs of events that occurred in the past, the last one was chosen as a worst-case scenario unlikely to recur frequently. These scenarios will serve to calculate run-up heights along the northern coast of Haiti, in particular in the densely populated, low-lying coastal city of Cap Haitien, and to provide quantitative insight into the question of the source of the 1842 northern Haiti earthquake.

2 GEOLOGICAL SETTING

The northern Caribbean islands mark the boundary between the large North American plate to the north and the Caribbean plate to the south (Fig. 1). Geodetic measurements with the Global Positioning System (GPS) show that the relative motion between the two plates currently occurs at 19 mm yr^{-1} in a N80E direction (Fig. 1a, DeMets *et al.* 2000). This direction is quasi-constant along the plate boundary so that, as its trace changes direction from west to east, the tectonic regime transitions from strike-slip along the Cayman Trough, to oblique subduction in Puerto Rico, then to a classic frontal subduction in the Lesser Antilles (Mann *et al.* 2002).

At the longitude of the island of Hispaniola, the oblique relative motion between the Caribbean and North American plates is partitioned between plate-normal convergence along the offshore North Hispaniola thrust fault, and plate-parallel strike-slip motion on the ∼E–W trending Septentrional and Enriquillo faults in the northern and southern parts of the island (Fig. 1). Block modeling of GPS velocities in Hispaniola indicates that these faults are all locked and building up elastic strain at a rate of 1–3 mm yr^{-1} (North Hispaniola fault), 10–12 mm yr^{-1} (Septentrional fault) and 5–7 mm yr^{-1} (Enriquillo fault; Calais *et al.* 2002; Manaker *et al.* 2008; Calais *et al.* 2010; Benford *et al.* 2012). All three main faults are associated with large historical earthquakes responsible for significant destruction: in 1701 and 1751 in southern Haiti possibly on the Enriquillo fault system, in 1842 and 1887 in northern Haiti possibly on the Septentrional fault (Scherer 1912; Tanner & Shepherd 1997; McCann 2006), and in 1943–1956 on the North Hispaniola fault offshore the northeastern Dominican Republic (Dolan & Wald 1998).

The 1842 May 7 earthquake is central to this study. It struck the northern coast of Haiti at 17:00 local time, with an estimated magnitude varying amongst authors from 8.0 (McCann 2006) to 7.6 (ten Brink *et al.* 2011). It caused extensive damage in northern Hispaniola, with macroseismic intensities up to IX in Môle Saint Nicolas, Port-de-Paix, Cap Haitien, and Fort Liberté in Haiti, as well as in Santiago in the Dominican Republic according to an interpretation of newspaper reports by ten Brink *et al.* (2011). Shaking was felt in Cuba (intensity of IX), Jamaica, Puerto Rico, almost all the Lesser Antilles, New Orleans and throughout the southeastern U.S. (Ardouin 1856; Heck 1947). Destructive effects were reported at Grand Turk and St Thomas (Virgin Islands), where houses collapsed. The earthquake was also felt on ships in the roadsteads (Mallet 1855; O'Loughlin & Lander 2003). The earthquake destroyed many buildings in Cap Haitien, killing about 5000 people in that city, half of its population at the time (Scherer 1912). It also caused severe damage in the less populated cities of Port-de-Paix to the west (200 fatalities for 3000 inhabitants) and Santiago to the east in the Dominican Republic (200 fatalities for 30 000 inhabitants). No significant damage was reported in the other major population centers of the time in Port-au-Prince, Léogane and Jacmel in the southern part of the island.

The same earthquake was accompanied by a tsunami that killed ∼300 people with wave heights of 2 m along the northeastern Haitian coast. A maximum run-up of 4.6 m was reported in the city of Port-de-Paix (Table 1; Scherer 1912; O'Loughlin & Lander 2003), where the tsunami first manifested itself as a 60–100 m sea retreat followed by a returning wave that flooded the city up to ∼400 m inland (Madiou 1843), suggestive of a leading depression *N*-wave (Tadepalli & Synolakis 1996). In Cap Haitien, the ocean inundated the business streets of the seafront (Ardouin 1856). According to a report by Demesvar Delorme, the low elevation neighborhood of the old military headquarters (∼170 m inland the north part of Cap Haitien) may have been flooded, but the location of the depicted scene is vague. Fort Liberté, whose harbor and city were built in a sheltered bay protected by guarded outpost forts at its entrance, also experienced the tsunami (Lander 1997). In this area, the Massacre and Yaque rivers both overflowed their banks, so that the two rivers became one and flooded the neighboring countryside (Ardouin 1856).

Far field effects were reported in the United States (then Danish) Virgin Islands to the east (∼3.1 m run-up in St John) and in Grand Turk to the north, though information from historical archives is limited. There are no known reports of tsunami noted to the west and south in Cuba, Jamaica or along the southern peninsula of Haiti. Small waves were noticed at various places along the Atlantic coast of North America (Scherer 1913), which, if true, would indicate that the tsunami spread at basin scale far northward. The hypothesis of a teletsunami also seems to be supported by wave heights reported far to the south and east throughout the Lesser Antilles according to Lander (1997), with 0.9 m at Basse-Terre (Guadeloupe), 1.8 m at Bequia Island (Grenadines), and waves carrying away floatable objects down to Gouyave (former Charlotte Town) in Grenada. The accuracy of some of these reports is however questionable. The degree of confidence we can grant to water heights from historical archives is indeed difficult to assess, as shown for example by Ambraseys et Synolakis (2010) in their critical revision of tsunami catalogs for the eastern Mediterranean sea.

The 1842 earthquake is commonly thought to have ruptured the Septentrional fault offshore northern Haiti because it is the known active fault closest to the affected area (McCann 2006; Tabrez Ali *et al.* 2008; ten Brink *et al.* 2011). Damage location and importance from historical reports contain useful information on the rupture location, but are likely biased by the location of the main population centers of the time and by the local subsurface geology. ten Brink *et al.* (2011) interpreted these felt reports to compile a dataset of estimated seismic intensities, and estimated the 1842 rupture as extending ∼300 km along the Septentrional Fault,

Table 1. Historical tsunami observation for the 1842 and 1946 events (Scherer 1912; Heck 1947; Lander 1997; O'Loughlin & Lander 2003).

1842 May 7 earthquake			1946 August 4		
Location		Tsunami observation	Location		Tsunami observation
Haiti	Môle St-Nicolas	2 m	Dominican Republic	Northern coast	4.6 m
	Port-de-Paix	4.6 m		Matancitas	2.4 m
	Turtle Island	2 m		Julia Molina	4–5 m
	Cap Haitien	2 m		Cabo Samana	4–5 m
	Fort-Liberté	2 m	San Juan		0.66 m
Dominican Republic	Santo Domingo	1.6 m	Puerto Rico		effects
	Western Cibao Valley	effects	Bermuda		effects
US Virgin Islands	St John, St Thomas	3.1 m	USA	Daytona beach	effects
Lesser Antilles	Basse-Terre	0.9 m		Atlantic City	effects
	Bequia island	1.8 m			
	Grand Turk	effects			
	Atlantic coast	small waves			
Jamaica	Spanish town	negligible effects			

well into the present Dominican Republic, along the whole Cibao Valley, up to the vicinity of San Francisco de Macoris. However, this interpretation is not without controversy, since the large intensities reported near and to the east of Santiago (including at La Vega, cited by ten Brink *et al.* (2011) as a high-intensity locale) could result from site effects locally amplifying ground accelerations. These communities were built in the middle of a basin featuring soft sedimentary layers (Chiesa & Mazzoleni 2001) that classically trap and amplify seismic waves (e.g. Bard & Bouchon 1985; Su *et al.* 1992; Joyner 2000; Hough *et al.* 2010). Note in particular that such effects can take place at epicentral distances of several hundred km, a famous example being the significant destruction incurred in Mexico City from earthquakes at a distant subduction zone (e.g. Campillo *et al.* 1989). Further, Prentice *et al.* (2013) disputed ten Brink *et al.*'s (2011) interpretation on the basis of the absence of post-1492 surface rupture on the Septentrional Fault, based on a number of palaeoseismic trenching experiments carried out in that province (Prentice *et al.* 2003). In reply, ten Brink *et al.* (2013) pointed out that the coarse geographical sampling of the trenches could have missed a heterogeneous rupture.

In this context, the assumption that the 1842 rupture took place on the Septentrional fault is not supported by direct evidence of surface rupture. Since the fault runs at sea further west, where the highest intensities were reported, the association of the 1842 earthquake with the Septentrional Fault remains speculative. Consequently, it is legitimate to entertain a competing model where the 1842 shock would have taken place as a subduction event on the offshore North Hispaniola thrust fault (Fig. 1). This structure was responsible for the 1946 August 4 $M = 8.1$ earthquake farther east (Dolan & Wald 1998), an event that triggered a regional-scale tsunami with waves up to 4–5 m high along the northern coast of the Dominican Republic. The associated inundation caused about 100 fatalities in Bahia Escocesa in the northeastern Dominican Republic (Lynch & Bodle 1948), with effects reported in Puerto Rico, Bermuda, Florida and New Jersey (Table 1; O'Loughlin & Lander 2003).

3 SEISMIC SOURCES TESTED

We address both the issues of tsunami hazard in northern Haiti and the source of the 1842 earthquake modelling three scenarios consistent with the seismotectonic context of the region and with its known historical earthquake and tsunami history, based on the recommendations of the 2013 IOC Meeting of Experts (IOC Workshop Report No. 255; Table 3). Many other choices are possible, but the sources chosen here are particularly relevant, because they are likely the most damaging for northern Haiti. Model results can therefore provide a basis for developing conservative maps of run-up heights that can be transferred, with added factors of safety, into practical implementation for tsunami preparedness and protection.

Scenario 1 corresponds to a $M_w = 8.0$ strike-slip earthquake on the Septentrional Fault, with a rupture involving two segments extending from the southeastern tip of Cuba to the entrance of the Cibao Valley in the Dominican Republic, covering a total length of 330 km. This geometry is consistent with offshore surveys that document the linearity of these two segments with a slight change of direction at the longitude of the Tortue Channel (Calais *et al.* 1998). We model the rupture as a vertical plane with uniform 5 m coseismic slip and pure left-lateral strike-slip movement. It is intended to simulate the 1842 Haiti earthquake in its common interpretation as a rupture of the Septentrional Fault offshore northern Haiti. We do not consider an expanded model of rupture along the Septentrional Fault, extending as far east as Santiago De Los Caballeros and San Francisco De Macoris (ten Brink *et al.* 2011), since this additional rupturing on land would not contribute significantly to tsunami genesis, even though a greater fault length could be associated with a larger seismic slip.

Scenario 2 corresponds to a $M_w = 8.1$ thrust earthquake on the offshore North Hispaniola thrust fault system. We model it as a single-segment rupture with a simplified geometry derived from bathymetry and seismic reflection data (Dillon *et al.* 1992; Dolan & Wald 1998) as well as earthquake hypocenter depth distribution (Calais *et al.* 1992; Symithe *et al.* 2015). We use a 21° dip and a 190 × 60 km (length × width) rupture area with uniform 5 m coseismic slip and pure dip-slip reverse motion.

Scenario 3 corresponds to the worst-case, where the offshore North Hispaniola thrust fault would rupture from the southeastern tip of Cuba all the way through the western end of the 1946 earthquake rupture at the junction between the North Hispaniola and Puerto Rico trenches. The scenario consists of three segments, following a simplified geometry derived from offshore geophysics and earthquake depth distribution (Dillon *et al.* 1992; Dolan & Wald 1998; Calais *et al.* 1992; Symithe *et al.* 2015). We use a 21° dip and a total 618 × 59 km rupture area with uniform 10 m coseismic slip and pure dip-slip reverse motion, which corresponds to a $M_w = 8.7$ earthquake (Table 3). The width and dip of that thrust source imply that the surface projection of the down dip limit of the rupture reaches 55 km south of the North Hispaniola thrust fault, and thus

does not intersect the Septentrional fault at depth, consistent with the geometry proposed by Dolan & Bowman (2004).

Scenarios 1 and 2 can be considered analogous to two historical earthquakes: the former represents the 1842 source as proposed by most authors (McCann 2006; Tabrez Ali *et al.* 2008; Prentice *et al.* 2003, 2013), but not all (ten Brink *et al.* 2011). The latter is similar in moment release and geometry to the 1946 Dominican Republic earthquake but with an epicentre shifted westward offshore the northern coast of Haiti. Moment magnitudes where calculated using $M_w = (\log_{10} M_0 - 16.1)/1.5$ (Kanamori 1977) with $M_0 = \mu ULW$ (Aki 1967), where μ is the shear modulus (3.3×10^{11} dyn cm^{-2}), U the coseismic slip and L and W the length and width of the rupture plane, respectively (Table 3).

Clearly, these scenarios are a simplified version of many possible tsunami sources. One does not expect coseismic slip to be uniform or necessarily reaching the trench. Furthermore, our source parameters, and principally seismic slips, were derived using general scaling laws of earthquake similitude (e.g. Geller 1976), appropriately adapted to the case of strike-slip faulting (Scholz 1982). As such, we do not consider the possibility of slow seismic ruptures, as in the case of the so-called 'tsunami earthquakes' (Kanamori 1972), which could enhance the tsunamigenic potential relative to the high-frequency seismic spectrum controlling felt intensities. There is certainly a need for further exploration of these parameters. However, in the absence of additional constraints from historical or instrumental tsunamigenic earthquakes in the region, and in the spirit of delivering realistic worst-case scenarios, we decided to use the simplified rupture sources described above, all reaching the seafloor.

One must also note that our models are strictly dislocative, that is do not consider the effect of submarine landslides triggered by the earthquake. Underwater mass movements have been suggested as significant generators of tsunamis in the near field for more than 100 yr (e.g. Verbeek 1900; Gutenberg 1939), and recently documented as major contributors to tsunami hazard (e.g. Synolakis *et al.* 2002; Okal *et al.* 2009). Indeed, all the tsunami victims of the 2010 January 12 Haiti earthquake resulted from a wave caused by a coastal landslide at Petit Paradis (Hornbach *et al.* 2010; Fritz *et al.* 2013). PGA studies for this event show that the main shock shaking was ~0.2 g in much of Port-au-Prince (corresponding to a VI MMI intensity), with peak accelerations ranging from 0.3 to 0.7 g at sites of strongest local amplification (i.e. up to a VIII MMI intensity; Hough *et al.* 2012). In the 1842 earthquake context, the MMI IX intensities reported along the Northern Haiti coastline would suggest accelerations on the order of 0.3 g (Murphy & O'Brien 1977), which, assuming sufficiently steep offshore slopes, would be in excess of the 0.1–0.2 g generally recognized as the threshold of stability for the triggering of landslides in benthic sediments (Keefer 1984).

4 TSUNAMI CALCULATION METHOD

The numerical method involves modelling of the initiation, propagation, and run-up of the tsunami waves. The computation of the initial seafloor perturbation responsible for the tsunami triggering uses coseismic static ground displacement for a uniform dislocation in an elastic half-space (Okada 1985), assumed to be instantaneously and fully transmitted to the water column.

Under the non-dispersive shallow water assumption, propagation in the deep ocean is solved through a finite difference scheme taking into account the non-linear terms of the depth-averaged hydrodynamical equations describing the conservation of mass (1) and momentum (2):

$$\frac{\partial (\eta + h)}{\partial t} + \nabla \cdot [\boldsymbol{v} (\eta + h)] = 0 \tag{1}$$

$$\frac{\partial \boldsymbol{v}}{\partial t} + (\boldsymbol{v} \cdot \nabla)\ \boldsymbol{v} = -g \nabla \eta + \mathbf{f}, \tag{2}$$

where h is the water depth, η the water elevation above mean sea level, $\boldsymbol{v}$ the depth-averaged horizontal velocity vector, g the scalar acceleration of gravity and $\mathbf{f}$ the combination of bottom friction and Coriolis forces, both of them being in general first-order in $\boldsymbol{v}$. These equations are solved using a Crank–Nicolson method centered in time, with an upwind scheme in space (see Hébert *et al.* (2001) for more details on the numerical method).

The main drawback of the finite difference method is the constant spatial increment over the whole computation grid. To deal with shoaling and resonance effects of the tsunami waves, detailed bathymetric grids are used for the precise modelling of the coastline response in bays and harbours. To this end we calculated wave propagation on four successive levels of nested grids of increasing resolution close to the shore, built using available bathymetric data (Fig. 2). The two lower resolution grids use the GEBCO World Bathymetry (resolution from 30 inches to 200 m, Table 2). The two higher resolution grids zoom in on the northern Haitian coastline to enclose the Cap Haitien area (40 m and 10 m cell-size grid, respectively, Table 2), and include the topography close to the shores. We built these finer grids from digitized, georeferenced and interpolated nautical bathymetric charts (NGA charts 26141, 26142 and 26147; Fig. 2).

Open free boundary conditions are prescribed to the boundaries of the grid covering the Caribbean basin, and wave heights along the boundaries of a fine grid are spatially interpolated at each time step from the value computed in the coarse grid containing the fine grid. In addition, the method takes into account the inundation of the coastal areas and allows us to compute run-up values thanks to the topography provided within the first emerged tens of meters of the finer grids. Numerically, this is handled by an extrapolation of the results from dry to wet nodes at the dynamic shoreline. This tsunami modelling code has been used worldwide and has proven its efficiency, especially in the Pacific through the simulation of waves triggered by historical and great earthquakes of the last decades were ample data is available to validate the simulations (e.g. Hébert *et al.* 2007, 2009; Reymond *et al.* 2012). The code is also implemented on multiprocessor computers within the French tsunami warning centre (CENALT), and used as an 'on-the-fly' operational tsunami modelling tool (Schindelé *et al.* 2015).

5 RESULTS

5.1 Overview

We computed the coseismic vertical displacement for each tested seismic source and for each grid level (Fig. 3 – bottom). As we are using uniform coseismic fault slip distribution, the coseismic motion of the ocean bottom, and hence the initial values of our simulations, are themselves spatially slowly varying, and their amplitudes increase smoothly from source 1 to 3. For scenario 1, the coseismic displacement does not exceed ±20 cm, as expected for pure strike-slip movement along the Septentrional Fault. Scenarios 2 and 3, both involving pure reverse slip reaching the seafloor, involve large coseismic seafloor motion with amplitudes from ±2 to

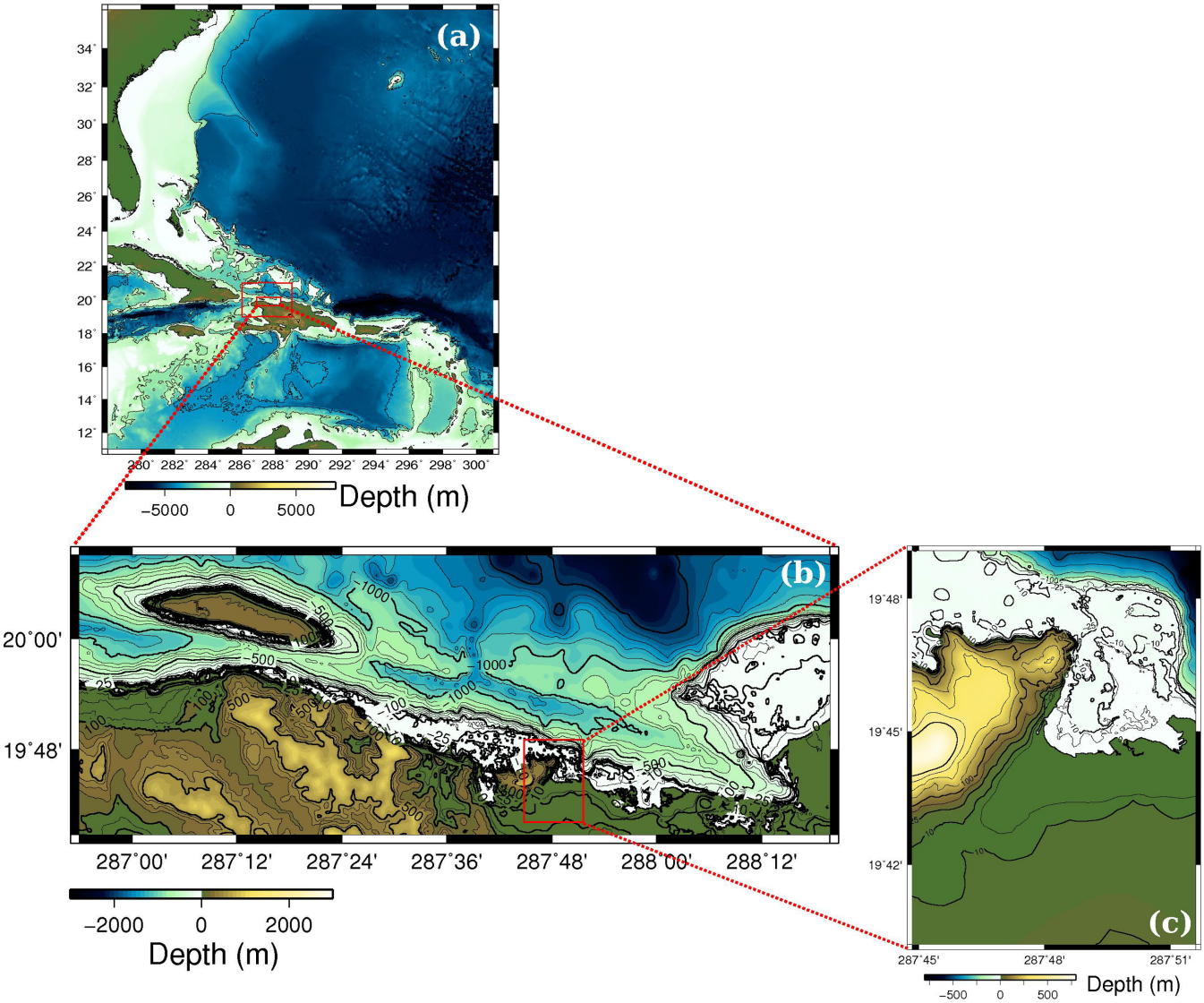

Figure 2. Nested bathymetry grids (four levels of resolution, Table 2) used for the tsunami modeling. (a) 30 s GEBCO grid. Red rectangles indicate the 200-m and 40-m-resolution daughter grids boundaries; (b) 40-m-resolution grid for the northern Haiti coast (digitized from charts); (c) 10-m-resolution grid for the Cap Haitien area (digitized from charts).

Table 2. Set of nested bathymetric grids of increasing resolution used for the tsunami modelling (four levels of imbrication from 0 to 3). The cell-size from one grid to its daughter respects a step of ∼4, so that the shoaling effect is well reproduced and the wavelengths are sampled properly.

Grid Nb	Lon min (°)	Lon max (°)	Lat min (°)	Lat max (°)	Cell-size	nx ∗ ny	Origin
0	–81.9958	–58.9958	10.9958	35.9958	30 sec	2761 ∗ 3001	30 s GEBCO
1	–74	–71.1002	19	20.9998	200 m	1612 ∗ 1112	30 s GEBCO resampling
2	–73.1	–71.67	19.6471	20.15	40 m	3764 ∗ 1324	From charts
3	–72.2525	–72.14	19.67	19.8179	10 m	1250 ∗ 1644	From charts

±4 m, respectively. Such seafloor vertical displacements obviously have the potential to trigger energetic tsunamis, as observed after a number of subduction events of similar magnitude (e.g. Satake & Atwater 2007). These values are comparable to vertical coseismic uplifts inferred for other events, such as the $M_w = 8.1$, 1995 Antofagasta subduction earthquake (Ruegg *et al.* 1996; Hébert *et al.* 2001), the $M_w = 9.0$, 1700 Cascadia earthquake (Satake *et al.* 2003), or the 2005 and 2007 Sumatra events (Konca *et al.* 2007; 2008). Northern Haiti and Dominican Republic are however in a more perilous situation because of the proximity of the trench to the coast (30–50 km), a value at the very low end of all subduction zones where the trench/coast distance typically ranges from 100 to 300 km. This setting would obviously result is a very short lead-time for response.

Fig. 3(top) shows the resulting wave heights for the first 12 hours following the earthquake at basin scale. The wide range of initial coseismic seafloor motion leads to significant differences in tsunami impact in the Caribbean basin, especially along the northern Haitian coast. The tsunami generated by scenario 1 is limited in amplitude (<0.5 m) and propagation, as expected given the small vertical coseismic seafloor motion. The wave does not reach beyond the

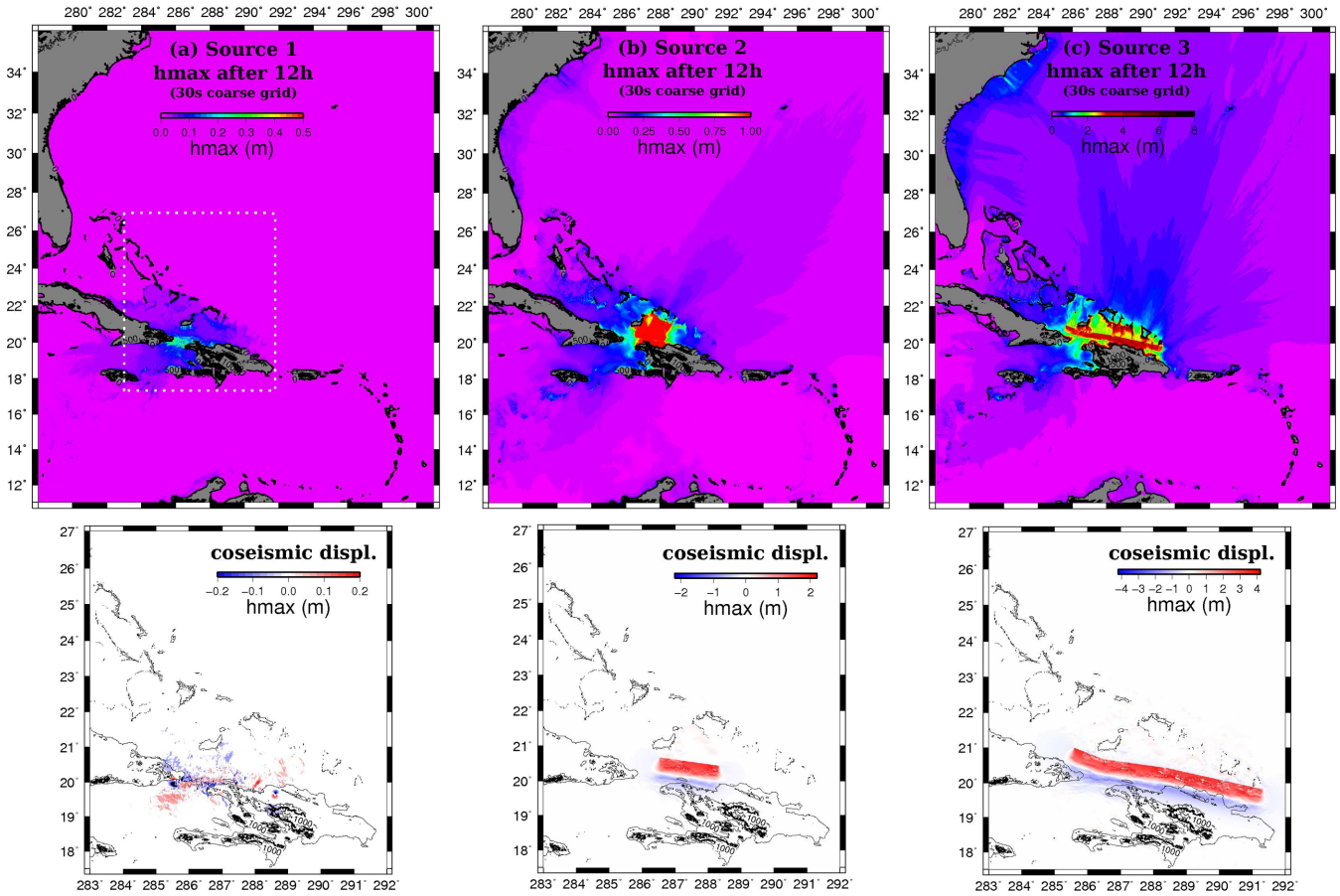

Figure 3. Bottom: coseismic vertical displacements computed with the Okada elastic dislocation model (1985) displayed for the three different seismic sources tested, (a) source 1, (b) source 2 and (c) source 3. Top: corresponding maximum water height after 12 hr of propagation in the 30 s resolution grid. The white dashed rectangle indicates the boundary of the coseismic vertical displacement maps.

Turk and Caicos Islands to the north and Jamaica to the south, with very low amplitudes (<0.1 m). The maximum tsunami amplitude, ~0.3 m, is obtained between Haiti and the eastern coast of Cuba. This scenario is therefore unlikely to explain the 1842 historical reports of tsunami impact in particular in the far field in the Virgin Islands and the Atlantic seaboard of North America.

Scenarios 2 and 3 generate widely larger tsunamis with open ocean wave heights up to 1 and 8 m, respectively (Figs 3b and c – top). The northern coast of Hispaniola is clearly the most impacted, with wave heights at least 5 times larger than in scenario 1. Our models show that such scenarios also generate a tsunami in the bay of Port-au-Prince, with smaller wave heights compared to the north coast of Haiti. Interestingly, in spite of such large amplitudes, the tsunami propagation is limited in spatial extent due to the Bahamas platform bathymetric high, which hinders propagation to the north. As a result, only a small fraction of the maximum tsunami energy reaches the north Atlantic coast, but coastal amplification effects leading to small waves heights are predicted within 12 hours of propagation. In these simulations, the Turk and Caicos Islands are severely impacted, as well as the southeastern tip of Cuba. We unfortunately lack historical data in these regions at the time of the 1842 event. Searching their historical archives may lead to crucial information on that event and on regional tsunami hazard in general. As the thrust fault system is oriented ESE-WNW, tsunami propagation is more restricted eastward, but waves of 25 cm to >1 m height reach Puerto Rico and the Virgin Islands (Figs 3b and c – top). The maximum wave height after 12 hours of propagation shows that the Lesser Antilles are also slightly impacted by the tsunami, albeit with weaker amplitudes. The southern coast of Hispaniola appears to be protected from significant impact.

5.2 Northern coast of Haiti

We now turn to the specific impact of these scenarios on the northern coast of Haiti. Fig. 4 compares maximum wave heights within 3 hr of the earthquake on a 40 m resolution grid along the entire coastline. Fig. 5 shows synthetic tide gauge time series at discrete locations chosen in areas of population exposure such as villages, bays or beaches, as well as places where historical tsunami observations were reported in 1842.

We observe that scenario 1 does not generate any observable run-up (Fig. 4a) and produces maximum wave amplitudes that do not exceed 50 cm at any location along the coast (Fig. 5, green curves). Wave amplitude observations of about 2 m reported in 1842 in several locations along the coast of northern Haiti are not consistent with such a scenario, unless they were caused by local submarine landslides triggered by the earthquake ground shaking.

Scenarios 2 and 3, on the contrary, lead to significant water height and run-up at a number of locations along the coast (Figs 4b and c). The tsunami signal is amplified strongly as a result of near-shore

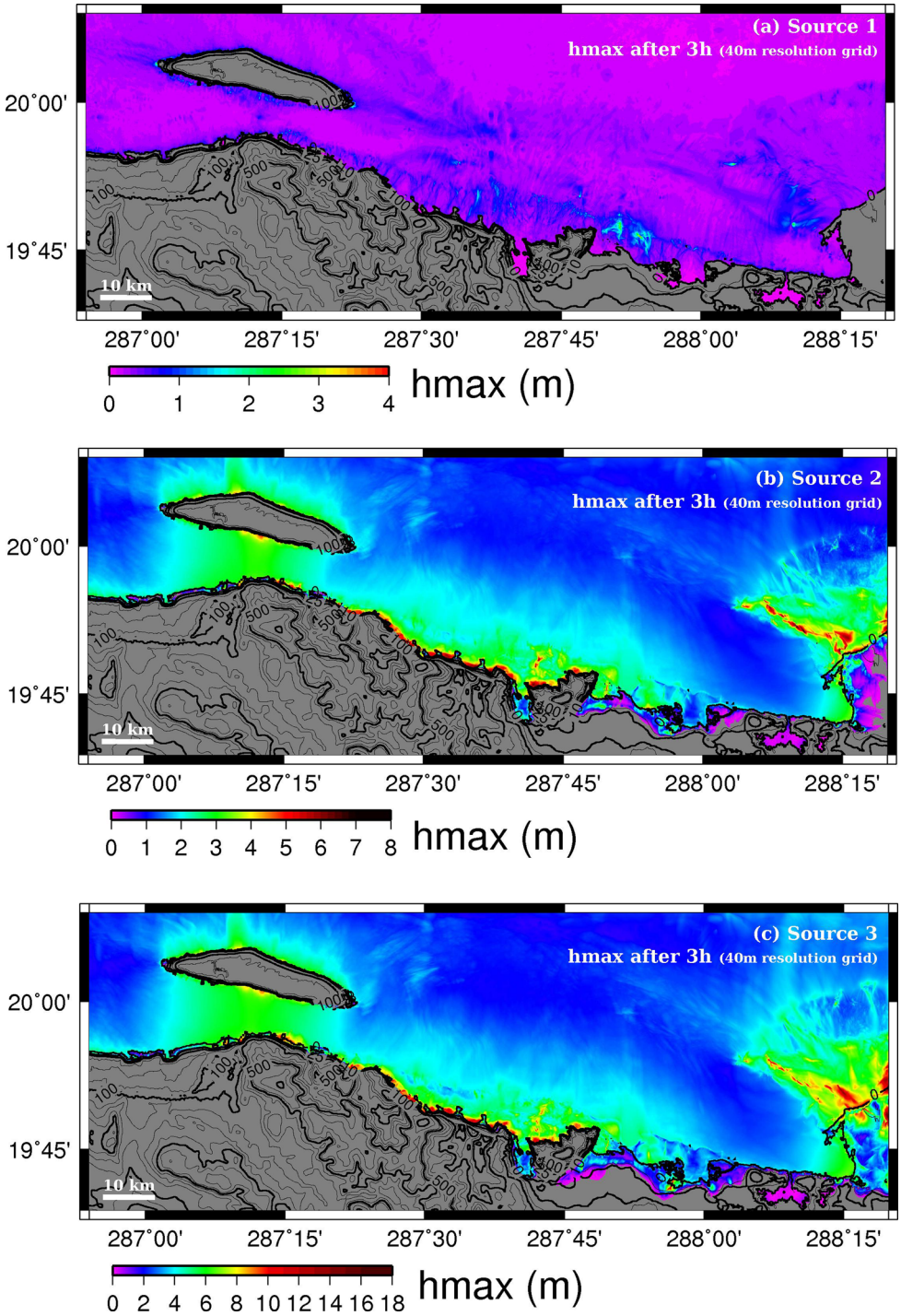

Figure 4. Maximum water height after 3 hr of propagation in the 40-m-resolution grid for (a) source 1, (b) source 2 and (c) source 3. Note that for the northern coast of Haiti, the 'worst case' scenario is provided by source 2.

bathymetric features present in the high-resolution grid used here (40 m). The model periods (10 min on average) and phases are consistent amongst scenarios. We also observe that all the sites of the north Haitian coast are exposed, with a first wave always very large and reaching the shoreline in less than 15 min. In the Tortue Channel (Port-de-Paix area), the wave height shows a second pulse with a 2 hr delay, most likely because of wave reflections due to the channel geometry. This result is important to include in the design of alert and emergency response strategies for northern Haiti.

Scenario 2 generates tsunami waves with up to 8 m of peak-to-trough amplitude in the first 3 hours along the western part of the coast (gauges 1–14, red curves, Fig. 5), reaching up to 12 m peak-to-trough at the shoreline in Port de Paix and Anse Gamelle. However, the model does not predict significant inundation along this coastal stretch, because of the steep offshore-onshore transition that characterizes the area. The near-shore coastal slope becomes smoother east of Cap Haitien, with coastal mangroves rather that steep cliffs, a near-shore plant marsh feature that favours flooding.

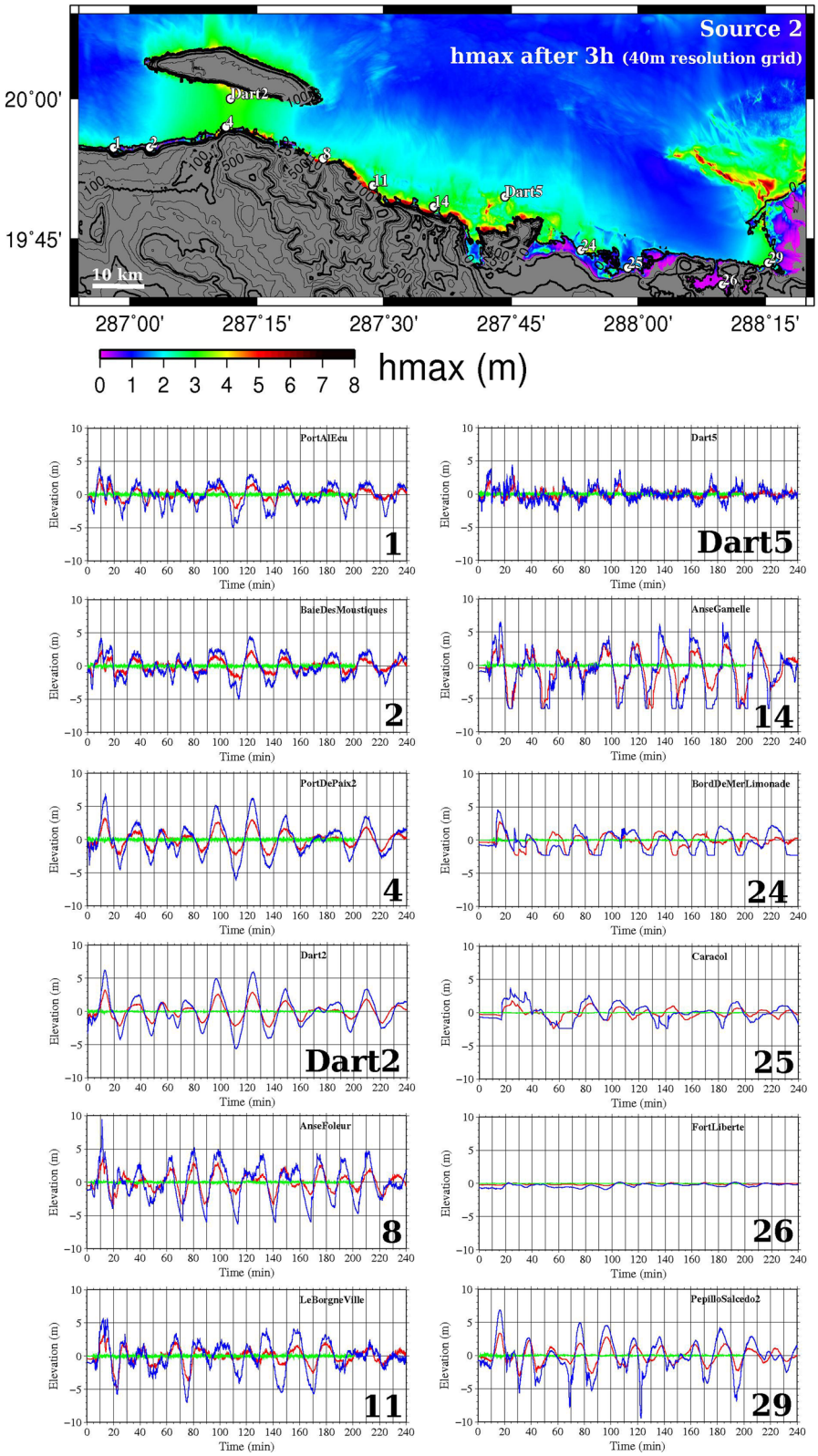

Figure 5. Synthetic tide gauge records at locations of interest along the northern coast of Haiti: (1) Port à l'Ecu, (2) Baie des Moustiques, (4) Port de Paix, (Dart2) deep sea point of interest, (8) Anse à Foleur, (11) Le Borgne, (Dart5) deep sea point of interest, (14) Anse Gamelle, (24) Bord de Mer Limonade, (25) Caracol, (26) Fort Liberté, (29) Pepillo Salcedo. Colours represent the three seismic sources tested in our simulations: red = source 2, blue = source 3, green = source 1. Map at the top shows the location of the synthetic gauges on top of the worst-case model result in the 40 m resolution grid (same as Fig. 4c).

Synthetic tide gauge records show lower wave amplitude values in this area (see Bord de Mer Limonade, Caracol and Pepillo Salcedo, gauges 24–25–29, red curves, on Fig. 5) but the tsunami penetrates between 2 and 4 km inland in the area of Bord de Mer Limonade and Caracol, with up to ~3 m of run-up locally (Figs 4b and 7). The predicted inundation is also significant at the Dominican Republic border (gauge 29, Fig. 5), with flooding of the present Montecristi National Park (Fig. 4b). On the opposite, the city of Fort Liberté is protected by the shape of its bay and is not expected to suffer any tsunami impact (gauge 26, Fig. 5). The extremely narrow funnel-spahe bay entrance raises questions about significant tsunami impact from any scenario, as shown in the case of a similar bay in Japan during the 2011 Tohoku earthquake (Shimozono *et al.* 2012). This questions the reliability of the 2 m wave heights reported in the area during the 1842 event. Either the outpost forts only could have been impacted this way, or the overflows of neighbouring rivers reported by Ardouin (1856) caused the flooding incorrectly reported as a tsunami wave. Worst-case scenario 3 is similar to scenario 2, but generates wave amplitudes approximately 1.5 m higher – or lower in case of drawdown – than scenario 2 (Fig. 4c and Fig. 5 – blue curves).

5.3 Cap Haitien area

The city of Cap Haitien is a historical landmark for Haiti and the region and presently an important national economic centre. Its present-day urban area extends over a surface of ~59 km^2, hosts an international airport, and concentrates approximately 250 000 inhabitants. We now focus on the impact of our three tsunami scenarios in this heavily populated city, where a large part of the population lives and works within a few meters of mean sea level.

Fig. 6 shows tsunami run-up in space and time at 6 locations in the bay of Cap Haitien and at some local landmarks (e.g. Cormier, Labadie) calculated using the highest resolution bathymetric grid (10 m resolution). As expected, scenario 1 does not produce any significant tsunami wave or run-up, with a maximum water height not exceeding 50 cm. However, scenarios 2 and 3 produce significant tsunami waves along the northern Haitian coast, resulting in widespread inundation in the city of Cap Haitien. The waves are guided by the Mapou River and spread to the south and east, but are blocked westward by the steep slope bounding Cap Haitien in that direction. The flooding covers the airport and almost the whole city and suburbs (Fig. 7), which raises the question of the establishment of accessible safety areas for the population, as well as access to the area for rescue personnel.

Scenario 2 generates a tsunami that penetrates up to 4 km inland with up to 4 m run-up (Fig. 6b). In the Cap Haitien bay, synthetic tide gauge data give wave amplitudes of 3–7 m peak-to-trough within the first 3 hr (gauges 21–22 – red curves, Fig. 6). To the west, the steep offshore-onshore transition precludes significant inundation, but the tsunami signal is strongly amplified, with peak-to-trough values reaching 8–9 m (gauges 16–20 – red curves, Fig. 6) and maximum water height of ~5 m (Fig. 6b). The only area to be flooded is the peninsula of Labadie which currently hosts an occasional day time stop for cruise ships (gage 17, Fig. 6); here the model predicts run-up of 2–3 m. Worst-case scenario 3 shows trends that are similar to scenario 2, with wave amplitudes up to 3–4 m higher and flooding spreading farther south and east in Cap Haitien (Fig. 6c).

6 DISCUSSION

6.1 The 1842 event is not well explained by scenario 1

Our calculations show that a tsunami triggered by a $M_w = 8.0$ strike-slip earthquake on the Septentrional fault offshore Haiti alone does not explain the wave amplitudes described in the 1842 historical records. This holds both in the near field with reports of 2 m wave heights at several locations and maximum run-up of 4.6 m in Port-de-Paix, and in the far field with reports in the Virgin Islands, Bahamas and along the Atlantic coast of North America. Although the reliability and accuracy of these historical reports is difficult to assess, they do not appear to be consistent with the prediction of a strike-slip source that leads to 0.5 m high waves at most. This low value is not consistent either with a tsunami whose origin would be the 1842 strike-slip source proposed by ten Brink *et al.* (2011), in which the Septentrional fault ruptures through the whole Cibao Valley in the Dominican Republic, a possibility refuted by Prentice *et al.* (2013) on the basis that no post-1492 surface rupture exists on the Septentrional fault in the central Cibao Valley east of Santiago.

If the 1842 earthquake did rupture the Septentrional fault north of Haiti, then ground shaking must have triggered a number of submarine landslides in order to obtain wave heights in agreement with historical observations, at least in the near field. The NE Caribbean contains regions of unstable seafloor associated with a primarily strike-slip tectonic context that have previously created tsunamigenic submarine landslides or slumps triggered by earthquake shaking (McCann 2006), as in the case of the 2010 Haiti event for instance (Hornbach *et al.* 2010; Fritz *et al.* 2013). Thus, one or several submarine landslides accompanying the 1842 earthquake could have strengthened the tsunami waves heights along the northern coast of Haiti. However, this hypothesis cannot explain far field observations in Puerto Rico or the U.S. Atlantic coast, as the combined effect of the earthquake and landslides would have remained local (e.g. Okal *et al.* 2009; Satake & Tanioka 2003).

Alternate explanations must therefore be proposed to reconcile reported wave heights with a rupture of the Septentrional fault. For instance, the rupture plane in scenario 1 is taken vertical with pure strike-slip motion, while there is evidence further east in the Cibao Valley that the Septentrional fault has a slight dip to the north with a reverse component (Calais *et al.* 1992). Given the regional-scale transpressional tectonic context throughout Hispaniola, earthquake ruptures can combine both strike-slip and dip-slip components, as evidenced by the 2010 January 12, Haiti earthquake whose moment release resulted from 1/3 dip-slip and 2/3 strike-slip motion (Calais *et al.* 2010; Hayes *et al.* 2010). The Septentrional fault trace offshore northern Haiti is however very linear, indicative of a nearly vertical dip. There is no evidence of significant splay faults that could have accounted for substantial reverse motion either in older offshore data (Calais *et al.* 1998) or in more recent data from a detailed bathymetric survey offshore northern Haiti (de Lépinay, personal communication, 2014).

6.2 The 1842 event is better explained by a variant of scenario 2

Altogether, the near and far field historical reports for the 1842 event appear in better agreement with a tsunami generated by a seismic source on the North Hispaniola thrust fault system offshore northern Haiti as modelled in scenario 2. Modelled water heights are consistent with reported historical values along the northern Haitian coast, despite a slight general overestimation in the simulations. In

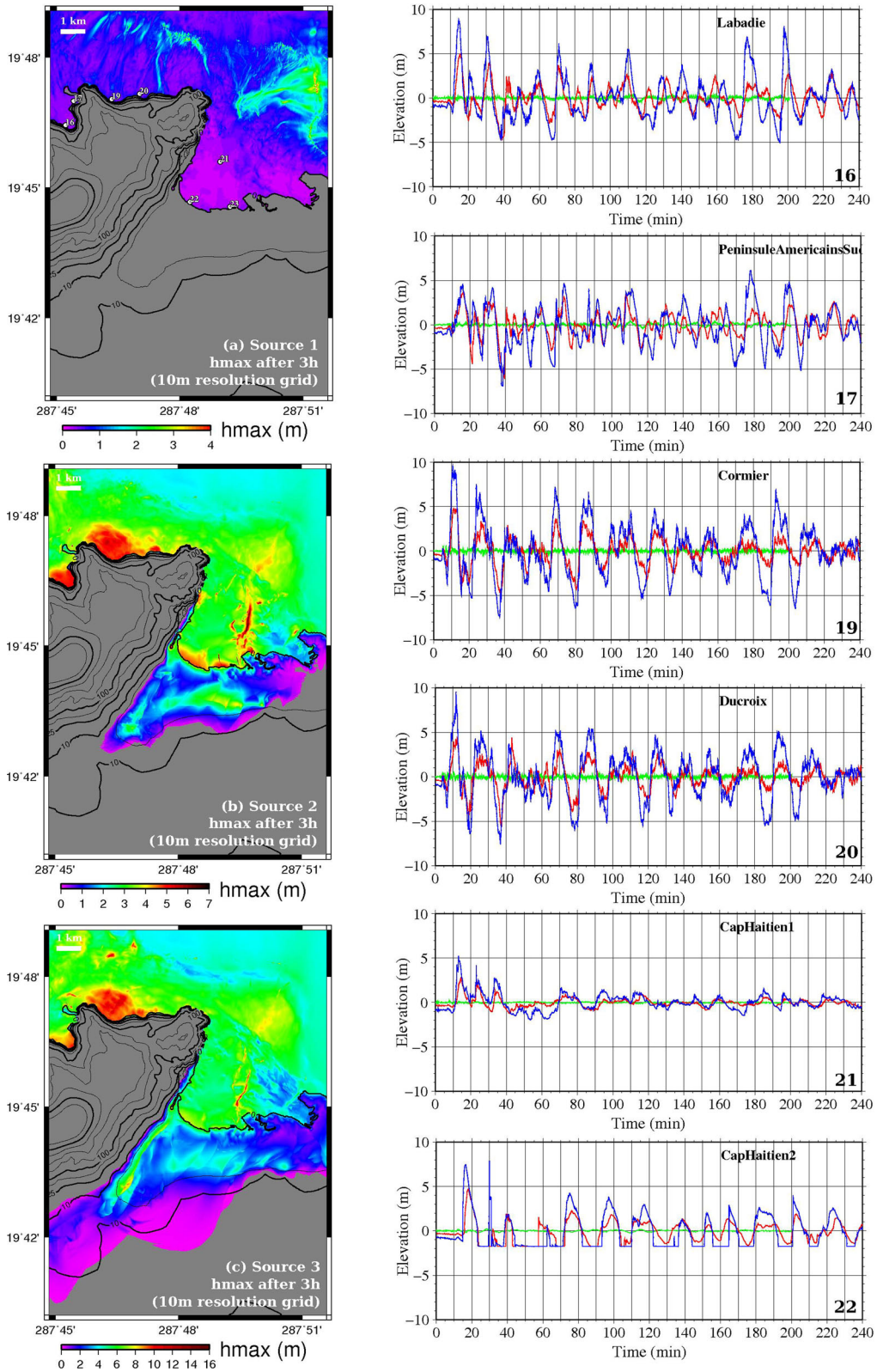

Figure 6. Left column: maps of maximum water height after 3 hr of propagation in the 10 m-resolution grid for (a) source 1, (b) source 2, and (c) source 3. Right columns: synthetic tide gauge records at locations of interest in the Cap Haitien area: (16) Labadie city, (17) Labadie peninsula, (19) Cormier, (20) Ducroix, (21) Cap Haitien, bay, (22) Cap Haitien, coast. Colors represent the three seismic sources tested in our simulations: red = source 2, blue = source 3, green = source 1.

Figure 7. Maximum flooding extent resulting from our calculation reported on the GoogleEarth image of Cap Haitien [left] and of the Caracol development zone [right] (data SIO, NOAA, US Navy, NGA, GEBCO. Image © 2015 DigitalGlobe © 2015 Google). Solid red line: inundation limit for scenario 2; dashed black line: inundation limit for scenario 3.

the area of Bord de Mer Limonade, Caracol and Fort-Liberté (at the entrance of the lagoon), calculations indicate maximum wave heights of 2–3 m at the shoreline (Fig. 4b), in good agreement with historical reports (Table 1).

By contrast, the tsunami amplification predicted by scenario 2 in the bay of Cap Haitien with up to 4 m of flow depth and the flooding of the city is uncertain to have occurred in 1842 (Fig. 6b) as it relies on a single witness report of water reaching a vague location in the northern part of the city. Similarly, there are no historical reports of waves higher than 2 m between Labadie and Anse-à-Foleur, whereas simulations show the strongest amplification along the North Haiti coast with maximum water heights reaching ~6 m in some coves (Fig. 4b), a result of the steep near shore bathymetric slope along this stretch of the northern Haiti coast. The lack of historical records could simply be an observational bias due to the fact that this area was quite deserted in the mid-19th century, except for the city of Port-de-Paix and its close surroundings where the 4.6 m reported wave height is well fit by the simulations with near shore amplification. It could also result from complexities of the earthquake rupture, obviously extremely simplified in the simulations.

A tsunami triggered by the offshore thrust fault also propagates farther north and east/south-east at basin scale, which is in general agreement with the admittedly imprecise 1842 far-field effects reported (Figs 3a and b, Table 1). Detailed bathymetry would be needed to evaluate the response of individual bays in Guadeloupe and Grenada and evaluate their amplification potential, in particular at the location where dubious observations were reported (e.g. high values reported at Deshaie and Ste Rose, Table 1). The relatively minor effects reported along the Atlantic coast of North America, in spite of the proximity of the event, are well explained by the bathymetric barrier effect exerted by the Bahamas platform barrier (Fig. 3), which efficiently shields most of the Atlantic basin from significant wave heights. On the other hand, our simulations predict that tsunami waves triggered by scenario 2 would amplify in the Port-au-Prince bay, where no tsunami observations were reported in 1842. Also scenarios 1 and 2 both predict significant tsunami impact along the eastern tip of Cuba for which no historical report exists. Again, these differences may result from an observational bias or reflect complexities in the source and/or propagation that are not accounted for in our calculations. For instance, the heterogeneous coseismic slip distribution likely to have taken place in 1842, as well as its kinematics, but also a slight shift of the rupture plane westward or eastward, would significantly modify the areas where the tsunami energy would be directed. Also, the pure reverse motion source used here could have, in actuality, contained a significant amount of strike-slip or oblique motion, which would result in weakening the induced tsunami energy.

In summary, if one takes the historical reports listed in Table 3 at face value, and in the strict context of a purely dislocative source (i.e. excluding the role of possible—if not probable—triggering of underwater landslides), it appears more logical to associate the tsunami to a rupture, perhaps complex, of the north Hispaniola thrust fault. Given the importance of that particular event for improving our understanding of tsunami hazard in the region it seems that testing this hypothesis should receive significant research attention in the future. Two types of targets come to mind. First, there may be much to learn by systematically searching through historical archives of the time in particular in Cuba and in the Turk and Caicos islands. Secondly, and beyond the sole 1842 event, run-up maps on Fig. 3 provide useful guidelines on where tsunami deposits from large pre-historical events are most likely to be found. Palaeo-shoreline studies (e.g. coastal uplift, coral and microfossils dating, or archaeological signature) and palaeo-tsunami field surveys are key to better understanding the rupture parameters and magnitude of historical earthquakes (e.g. Shaw *et al.* 2008), as well as the recurrence interval of large-scale tsunamis, as shown, for example by the study of the 869 and 2011 tsunamis in Japan (e.g. Minoura & Nakata 1994; Minoura *et al.* 2001; Sugawara *et al.* 2012; Namegaya & Satake 2014).

6.3 Tsunami Hazard in Northern Haiti

Independently from the discussion on the 1842 source, the tsunami scenarios proposed here provide important elements for assessing tsunami hazard in northern Haiti. Scenario 1 is a rupture of the Septentrional fault, a definite possibility given the current tectonic

Table 3. Seismic sources parameters tested for the tsunami modelling, derived from three scenarios established by experts during the 2013 IOC meeting in Haiti (Intergovernmental Oceanographic Commission Workshop Report No. 255, 2013).

		Scenario 1		Scenario 2	Scenario 3		
		West segment	East segment	Central segment	West segment	Central segment	East segment
Source parameters	Location	73.636°W 19.998°N	72.088°W 19.812°N	72.602°W 20.3025°N	74.009°W 20.587°N	72.602°W 20.302°N	70.208°W 19.876°N
	M_w	8		8.1		8.7	
	Fault type	Strike-slip		Thrust		Thrust	
	Strike	91°	103°	98°	111°	98°	102°
	Dip	89°	89°	21°	21°	21°	21°
	Rake	0°	0°	90°	90°	90°	90°
	Depth	10 km	10 km	10.572 km	10.572 km	10.572 km	10.572 km
	Slip	5 m	5 m	5 m	10 m	10 m	10 m
	Fault plane dimensions	177 ∗ 20 km	151 ∗ 20 km	192 ∗ 59 km	109 ∗ 59 km	192 ∗ 59 km	317 ∗ 59 km
		328 ∗ 20 km				618 ∗ 59 km	

context, and appears the less damaging, although such an event would likely trigger a number of submarine landslides which could each create significant run up locally. Scenario 3, involving a segment of offshore thrust fault ∼620 km in length, is also the least likely given the magnitude of the resulting event, as well as the fact that it requires several distinct segments of that thrust system to rupture simultaneously. It is a worst-case scenario. However, this possibility cannot be discounted, as proven, for example by the 2004 Sumatra–Andaman earthquake, whose fault length extended over segments with differing azimuthal orientations and morphological structures. More generally, Ando (1975) has shown that large subduction zones which may appear as naturally fragmented into individual blocks or segments can support megathrust events rupturing one, a number of, or all such segments, in a highly unpredictable, and perhaps intrinsically random fashion. His model, initially developed for the Nankai Trough in Japan, has been generally upheld by palaeoseismic studies along many subduction zones (Nanayama *et al.* 2003; Cisternas *et al.* 2005; Kelsey *et al.* 2005) and has been used in the south China sea (Okal *et al.* 2011).

Scenario 2, if it was indeed the source of the 1842 earthquake, is unlikely to repeat in the short term as it would take more than 1600 yr to load the North Hispaniola thrust fault to the point of a M_w 8 earthquake at its slow ∼3 mm yr^{-1} elastic strain accumulation rate (Calais *et al.* 2010). Conversely, if the 1842 earthquake did not rupture the Septentrional fault, then that fault represents a much more significant hazard source in the short term than proposed, for instance, by Manaker *et al.* (2008) who calculated that it was only capable of a M_w 6.9 event today, assuming a major event took place in 1842. Since there are no reports of other large earthquakes in northern Haiti since 1492, one cannot exclude that the Septentrional fault has accumulated a slip deficit of at least 5 m in the past 500 yr at its ∼10 mm yr^{-1} elastic strain accumulation rate (Calais *et al.* 2010; Benford *et al.* 2012), equivalent to an earthquake with M_w 7.7, if released in a single event today.

Much remains to be learned on the palaeoseismological history of the region so that, in the absence of more accurate historical information, the tsunami scenarios described above should all be considered possible for the purpose of preparedness and response. The impact of scenarios 2 and 3 on the northern Haitian coast is very significant. With the current population distribution, exposure, and vulnerability, these scenarios would be devastating, if they were to unfold, in particular for the city of Cap Haitien (Fig. 7). In the absence of tsunami modelling, the U.S. National Tsunami Hazard Mitigation Program (NTHMP) recommends defining the evacuation zone 3 km inland or 10 m above sea level, unless there is historical evidence of larger events. The simulations described above show that these recommendations are not sufficient in northern Haiti, especially in the Cap Haitien area, where flooding can reach more than 4 km inland, and waves reach more than 10 m height in worst-case scenario 3. In the case of a tsunamigenic event triggered by the rupture of the North Hispaniola thrust fault, the first waves would hit the city within 10–15 min after the earthquake, and maximum amplitudes could reach 5 to 7 m at the coastline (gauge 22, Fig. 6). The short time-window poses a significant problem, since, even in the optimal hypothesis of perfect citizen awareness that strong and long ground shaking should be considered as a tsunami warning, it leaves little time for the population to reach safe elevations. A possible mitigation solution may be to build artificial pillared platforms, as was done, for example in Aonae, on Okushiri Island, Japan or large mounds, as is being considered, for example in Padang, Sumatra (http://geohaz.org/projects/sumatra.html). The guidelines for the design of structures for vertical evacuation from tsunamis now also contains a chapter on tsunami loadings for engineering design purposes (see http://www.fema.gov/media-library-data/documents/14708). In the area of Petite Anse (eastern part of the city), the modelled inundation propagates up to 4 km inland. It covers, in particular, the entire runway of the Cap Haitian international airport. Alternate transportation options should therefore be sought in order to ensure optimal access for rescue and evacuation operations in case of a significant tsunami. Even though our simulations must be considered conservative as friction caused by buildings is not taken into account, the flat topography of the densely populated Petite Anse neighbourhood (<5 m above sea level) implies that there is no safe area for the population to take shelter. Well-positioned vertical evacuation constructions appear to be the only viable option in that part of the city.

Run-up heights predicted by our models are also significant in the Caracol area, which is currently being developed as an industrial park to spur economic growth and to bring 65 000 jobs to this underserved region. Clearly, economic and urban development in the coastal regions of northeastern Haiti—the so-called Cap Haitien-Fort Liberté corridor—must take into account the significant tsunami hazard of the region in the planning and design of facilities, lifelines and lodging compounds.

7 CONCLUSION

The tsunami calculations presented here, based on realistic seismotectonic scenarios, allow us to quantify the level of hazard along the northern coast of Haiti. The hazard is very significant in the case of the rupture of the offshore North Hispaniola thrust fault, with local

amplifications due to bathymetry, for instance in the Port-de-Paix area, and significant run-up predicted to inundate most of the city of Cap Haitien. The short interval between the time of a tsunamigenic earthquake and the arrival of the waves at the coast imply that (1) the population must be educated to the fact that strong and long ground shaking *is* the tsunami warning in the near field, and (2) mitigation solutions possibly involve building artificial structures within the city where the population can quickly find safe refuge. The calculations presented here should also serve as first-order information for planning the economic development of the northern coast of Haiti. A number of projects are underway; it is unclear how many proactively account for natural hazards, tsunamis in particular, in their design and planning.

Our calculations also shed some light on the source of the 1842 earthquake. The historical reports available, when compared to the simulations run here, favour a rupture of the North Hispaniola thrust fault, although much uncertainty remains. If the 1842 earthquake did not rupture the Septrentional fault, then the section of that fault that borders the northern coast of Haiti is currently capable of at least a M_w 7.7 earthquake, much larger than previously thought, given its current elastic strain accumulation rate. This calls for a renewed research effort to investigate historical and palaeohistorical records of tsunamis in the region in order to better understand the hazard posed by offshore active faults in Haiti and the northeastern Caribbean in general.

ACKNOWLEDGEMENTS

We thank Herman Fritz and an anonymous reviewer for their thoughtful comments that helped improve this manuscript. This research was supported by the Yves Rocard joint research laboratory (ENS/CEA/CNRS). EC acknowledges support from NSF grant EAR-1045809.

REFERENCES

Aki, K., 1967. Scaling law of seismic spectrum, *J. geophys. Res.,* **72**(4), 1217–1231.

Ambraseys, N. & Synolakis, C., 2010. Tsunami catalogs for the Eastern Mediterranean, revisited, *J. Earthq. Eng.,* **14**(3), 309–330.

Ando, M., 1975. Source mechanism and tectonic significance of historical earthquakes along the Nankai Trough, Japan, *Tectonophysics,* **27,** 119–140.

Ardouin, B., 1856. Etudes sur l'histoire d'Haïti. Port-au-Prince. Ed, *Fardin,* **3**(Tome 11), 49–51.

Bard, P.Y. & Bouchon, M., 1985. The two-dimensional resonance of sediment-filled valleys, *Bull. seism. Soc. Am.,* **75**(2), 519–541.

Benford, B., DeMets, C. & Calais, E., 2012. GPS estimates of microplate motions, northern Caribbean: evidence for a Hispaniola microplate and implications for earthquake hazard, *Geophys. J. Int.,* **191**(2), 481–490.

Calais, E., Perrot, J. & De Lepinay, B.M., 1998. Strike-slip tectonics and seismicity along the northern Caribbean plate boundary from Cuba to Hispaniola, Special Papers – Geological Society of America, Vol. 326, pp. 125–142.

Calais, E., de Lépinay, B., Saint-Marc, P., Butterlin, J. & Schaaf, A., 1992. La limite de plaques décrochante nord caraïbe en Hispanolia; évolution paléogéographique et structurale cénozoïque, *Bulletin de la Société Géologique de France,* **163**(3), 309–324.

Calais, E., Freed, A., Mattioli, G., Amelung, F., Jónsson, S., Jansma, P. & Momplaisir, R., 2010. Transpressional rupture of an unmapped fault during the 2010 Haiti earthquake, *Nat. Geosci.,* **3**(11), 794–799.

Calais, E., Mazabraud, Y., de Lépinay, B., Mann, P., Mattioli, G. & Jansma, P., 2002. Strain partitioning and fault slip rates in the northeastern Caribbean from GPS measurements, *Geophys. Res. Lett.,* **29**(18), 3–1.

Campillo, M., Gariel, J.C., Aki, K. & Sánchez-Sesma, F.J., 1989. Destructive strong ground motion in Mexico City: Source, path and site effects during the great 1985 Michoacán earthquake, *Bull. seism. Soc. Amer.,* **79,** 1718–1735.

Chiesa, S. & Mazzoleni, G., 2001. Dominican Republic (Hispaniola Island, North-Eastern Caribbean): a map of morpho-structural units at a scale 1: 500.000 through LANDSAT^{TM} image interpretation, *Revista Geológica de América Central,* **25,** 99–106.

Cisternas, M. *et al.*, 2005. Predecessors of the giant 1960 Chile earthquake, *Nature,* **437,** 404–407.

DeMets, C., Jansma, P.E., Mattioli, G. S., Dixon, T.H., Farina, F., Bilham, R. & Mann, P., 2000. GPS geodetic constraints on Caribbean-North America plate motion, *Geophys. Res. Lett.,* **27**(3), 437–440.

Dillon, W.P., Austin, J.A., Scanlon, K.M., Edgar, N.T. & Parson, L.M., 1992. Accretionary margin of northwestern Hispaniola: morphology, structure and development of part of the northern Caribbean plate boundary, *Mar. Petrol. Geol.,* **9**(1), 70–88.

Dolan, J.F. & Bowman, D.D., 2004. Tectonic and seismologic setting of the 22 September 2003, Puerto Plata, Dominican Republic earthquake: implications for earthquake hazard in northern Hispaniola, *Seismol. Res. Lett.,* **75**(5), 587–597.

Dolan, J.F. & Wald, D.J., 1998. The 1943–1953 north-central Caribbean earthquakes: Active tectonic setting, seismic hazards, and implications for Caribbean-North America plate motions, *Geol. Soc. Am. Spec. Pap.,* **326,** 143–169.

Engdahl, E.R., van der Hilst, R. & Buland, R., 1998, Global teleseismic earthquake relocation with improved travel times and procedures for depth determination, *Bull. seism. Soc. Am.,* **88** (3), 722–743.

Frankel, A., Harmsen, S., Mueller, C., Calais, E. & Haase, J., 2011. Seismic hazard maps for Haiti, *Earthq. Spectra,* **27**(S1), S23-S41.

Fritz, H.M., Hillaire, J.V., Molière, E., Wei, Y. & Mohammed, F., 2013. Twin tsunamis triggered by the 12 January 2010 Haiti earthquake, *Pure appl. Geophys.,* **170**(9–10), 1463–1474.

Geller, R.J., 1976. Scaling relations for earthquake source parameters and magnitudes, *Bull. seism. Soc. Am.,* **66,** 1501–1523.

Gutenberg, B., 1939. Tsunamis and earthquakes, *Bull. seism. Soc. Am.,* **29,** 517–526.

Hayes, G.P. *et al.*, 2010. Complex rupture during the 12 January 2010 Haiti earthquake, *Nat. Geosci.,* **3**(11), 800–805.

Hébert, H., Heinrich, P., Schindelé, F. & Piatanesi, A., 2001. Far-field simulation of tsunami propagation in the Pacific Ocean: impact on the Marquesas Islands (French Polynesia), *J. Geophys. Res.: Oceans,* **106**(C5), 9161–9177.

Hébert, H., Reymond, D., Krien, Y., Vergoz, J., Schindelé, F., Roger, J. & Loevenbruck, A., 2009. The 15th August 2007 Peru earthquake and tsunami: influence of the source characteristics on the tsunami heights, *Pure appl. Geophys,* **166,** 1–22.

Hébert, H., Sladen, A. & Schindelé, F., 2007. Numerical modeling of the great 2004 Indian Ocean tsunami: focus on the Mascarene Islands, *Bull. seism. Soc. Am.,* **97**(1A), S208–S222.

Heck, N.H., 1947. List of seismic sea waves, *Bull. seism. Soc. Am.,* **37,** 269–286.

Hornbach, M.J., Braudy, N., Briggs, R.W., Cormier, M.H., Davis, M.B., Diebold, J.B. & Templeton, J., 2010. High tsunami frequency as a result of combined strike-slip faulting and coastal landslides, *Nat. Geosci.,* **3**(11), 783–788.

Hough, S.E., Taniguchi, T. & Altidor, J.R., 2012. Estimation of peak ground acceleration from horizontal rigid body displacement: a case study in Port-au-Prince, Haiti, *Bull. seism. Soc. Am.,* **102**(6), 2704–2713.

Hough, S.E., Altidor, J.R., Anglade, D., Given, D., Janvier, M.G., Maharrey, J.Z. & Yong, A., 2010. Localized damage caused by topographic amplification during the 2010 M7.0 Haiti earthquake, *Nat. Geosci.,* **3**(11), 778–782.

Intergovernmental Oceanographic Commission, 2013. Earthquake and tsunami hazard in Northern Haiti: Historical events and potential sources (Meeting of experts), Paris, UNESCO, pp. 29 (IOC/2013/WR/255).

Joyner, W.B., 2000. Strong motion from surface waves in deep sedimentary basins, *Bull. seism. Soc. Am.,* **90**(6B), S95-S112.

Kanamori, H., 1972. Mechanism of tsunami earthquakes, *Phys. Earth planet. Inter.,* **6,** 346–359.

Kanamori, H., 1977. The energy release in great earthquakes, *J. geophys. Res.,* **82**(20), 2981–2987.

Keefer, D.K., 1984. Landslides caused by earthquakes, *Geol. Soc. Am. Bull.,* **95,** 406–421.

Kelsey, H.M., Nelson, A.R., Hemphill-Haley, E. & Witter, R.C.., 2005. Tsunami history of an Oregon coastal lake reveals a 4600-yr. record of great earthquakes on the Cascadia subduction system, *Geol. Soc. Am. Bull.,* **117,** 1009–1032.

Konca, A.Ö., Avouac, J.P., Sladen, A., Meltzner, A.J., Sieh, K., Fang, P. & Helmberger, D.V., 2008. Partial rupture of a locked patch of the Sumatra megathrust during the 2007 earthquake sequence, *Nature,* **456**(7222), 631–635.

Konca, A.Ö., Hjorleifsdottir, V., Song, T.R.A., Avouac, J.P., Helmberger, D.V., Ji, C. & Meltzner, A., 2007. Rupture kinematics of the 2005 M_w 8.6 Nias–Simeulue earthquake from the joint inversion of seismic and geodetic data, *Bull. seism. Soc. Am.,* **97**(1A), S307–S322.

Lander, J.F., 1997. Caribbean Tsunamis: an initial history, *Nat Haz,* **3,** 1–18.

Lynch, J.J. & Bodle, R.R., 1948. The Dominican earthquake of August, 1946, *Bull. seism. Soc. Am.,* **38,** 1–17.

Madiou, T., 1843. Histoire d'Haïti. Tome VII 1827–1843. Port-au-Prince : Ed. Deschamps, pp, 399–404.

Mallet, R., 1855. Catalogue of Recorded Earthquakes from 1606 B.C. to A.D. 1850, Part III, 1784 A.D. to 1842 A.D. Report of the 24th Meeting of the British Association for the Advancement of Science*,* John Murray, London, 326 pp.

Manaker, D.M., Calais, E., Fred, A.M., Ali, S.T., Przybylski, P., Mattioli, G. & De Chabalier, J.B., 2008. Interseismic plate coupling and strain partitioning in the northeastern Caribbean, *Geophys. J. Int.,* **174**(3), 889–903.

Mann, P., Taylor, F.W., Edwards, R.L. & Ku, T.L., 1995. Actively evolving microplate formation by oblique collision and sideways motion along strike-slip faults: an example from the northeastern Caribbean plate margin, *Tectonophysics,* **246**(1), 1–69.

Mann, P., Calais, E., Ruegg, J.C., DeMets, C., Jansma, P.E. & Mattioli, G.S., 2002. Oblique collision in the northeastern Caribbean from GPS measurements and geological observations, *Tectonics,* **21**(6), 7-1–7-13.

Mann, P., Prentice, C.S., Burr, G. & Taylor, F.W., 1998. Tectonic geomorphology and paleoseismology of the Septentrional fault system, Dominican Republic, *Geol. Soc. Am. Spec. Pap.,* **326,** 63–124.

McCann, W.R., 2006. Estimating the threat of tsunamogenic earthquakes and earthquake induced-landslide tsunami, in: *Caribbean Tsunami Hazard,* pp. 43–65, ed. Mercado Irrizary, A. & Liu, P.L-F., World Scientific Publishing.

Minoura, K. & Nakata, T., 1994. Discovery of an ancient tsunami deposit in coastal sequences of southwest Japan: verification of a large historic tsunami, *Island Arc,* **3**(1), 66–72.

Minoura, K., Imamura, F., Sugawara, D., Kono, Y. & Iwashita, T., 2001. The 869 Jõgan tsunami deposit and recurrence interval of large-scale tsunami on the Paciffic coast of northeast Japan, *J. Nat. Disaster Sci.,* **23,** 83–88.

Murphy, J.R. & O'Brien, L.J.., 1977. The correlation of peak ground acceleration amplitude with seismic intensity and other physical parameters, *Bull. seism. Soc. Am.,* **67,** 877–915.

Namegaya, Y. & Satake, K., 2014. Reexamination of the AD 869 Jogan earthquake size from tsunami deposit distribution, simulated flow depth, and velocity, *Geophys. Res. Lett.,* **41**(7), 2297–2303.

Nanayama, F., Satake, K., Furukawa, R., Shimokawa, K., Shigeno, K. & Atwater, B.F., 2003. Unusually large earthquakes inferred from tsunami deposits along the Kuril Trench, *Nature,* **424,** 660–663.

O'Loughlin, K.F. & Lander, J.F., 2003. *Caribbean Tsunamis: A 500-Year History from 1498–1998,* Vol. 20, Springer.

Okada, Y., 1985. Surface deformation due to shear and tensile faults in a half-space, *Bull. seism. Soc. Am.,* **75**(4), 1135–1154.

Okal, E.A., Synolakis, C.E. & Kalligeris, N., 2011. Tsunami simulations for regional sources in the South China and adjoining seas, *Pure appl. Geophys*., **168**(6–7), 1153–1173.

Okal, E.A., Synolakis, C.E., Uslu, B., Kalligeris, N. & Voukouvalas, E., 2009. The 1956 earthquake and tsunami in Amorgos, Greece, *Geophys. J. Int.,* **178**(3), 1533–1554.

Prentice, C.S., Mann, P. & Peña, L.R., 2013. Comment on: "Historical perspective on seismic hazard to Hispaniola and the northeast Caribbean region" by U. ten Brink *et al.*, *J. geophys. Res.: Solid Earth,* **118,** doi:10.1002/jgrb.50170.

Prentice, C.S., Mann, P., Peña, L.R. & Burr, G., 2003. Slip rate and earthquake recurrence along the central Septentrional fault, North American–Caribbean plate boundary, Dominican Republic, *J. geophys. Res.: Solid Earth,* **108**(B3), 1978–2012.

Reymond, D., Okal, E.A., Hébert, H. & Bourdet, M., 2012. Rapid forecast of tsunami wave heights from a database of pre-computed simulations, and application during the 2011 Tohoku tsunami in French Polynesia, *Geophys. Res. Lett.,* **39,** L11603, doi:10.1029/2012GL051640.

Ruegg, J.C., Campos, J., Armijo, R., Barrientos, S., Briole, P., Thiele, R. & Serrurier, L., 1996. The M_w 8.1 Antofagasta (North Chile) earthquake of July 30, 1995: first results from teleseismic and geodetic data, *Geophys. Res. Lett.,* **23**(9), 917–920.

Satake, K. & Atwater, B.F., 2007. Long-term perspectives on giant earthquakes and tsunamis at subduction zones, *Annu. Rev. Earth planet. Sci.,* **35,** 349–374.

Satake, K. & Tanioka, Y., 2003. The July 1998 Papua New Guinea earthquake: Mechanism and quantification of unusual tsunami generation, *Pure appl. Geophys.,* **160**(10–11), 2087–2118.

Satake, K., Wang, K. & Atwater, B.F., 2003. Fault slip and seismic moment of the 1700 Cascadia earthquake inferred from Japanese tsunami descriptions, *J. geophys. Res.: Solid Earth,* **108**(B11), 1978–2012.

Saurel, J.M., von Hillebrandt-Andrade, C., Crespo, H., McNamara, D. & Huerfano, V., 2014. Seismic monitoring capabilities of the caribbean and adjacent regions tsunami warning system, in *Proceedings of the EGU General Assembly Conference Abstracts* (Vol. 16, abstract 14969).

Scherer, J., 1912. Great earthquakes in the island of Haiti, *Bull. seism. Soc. Am.,* **2**(3), 161–180.

Scherer, J., 1913. Catalogue chronologique des tremblements de Terre ressentis dans l'île d'Haïti de 1551 à 1900, in *Bulletin Semestriel de L'Observatoire Météorologique du Séminaire-Collège St-Martial, Port-au-Prince, Haïti,* Juillet–Décembre 1913, pp. 147–151.

Schindelé, F. *et al.*, 2015. Implementation and challenges of the Tsunami Warning System in the Western Mediterranean, *Pure appl. Geophys,* **172**(3–4), 821–833.

Scholz, C.H., 1982. Scaling laws for large earthquakes: consequences for physical models, *Bull. seism. Soc. Am.,* **72,** 1–14.

Shaw, B. *et al.*, 2008. Eastern Mediterranean tectonics and tsunami hazard inferred from the AD 365 earthquake, *Nat. Geosci.,* **1**(4), 268–276.

Shimozono, T., Sato, S., Okayasu, A., Tajima, Y., Fritz, H.M., Liu, H. & Takagawa, T., 2012. Propagation and inundation characteristics of the 2011 Tohoku tsunami on the central Sanriku coast, *Coastal Eng. J.,* **54**(01), 1250004.

Su, F., Aki, K., Teng, T., Zeng, Y., Koyanagi, S. & Mayeda, K., 1992. The relation between site amplification factor and surficial geology in central California, *Bull. seism. Soc. Am.,* **82**(2), 580–602.

Sugawara, D., Goto, K., Imamura, F., Matsumoto, H. & Minoura, K., 2012. Assessing the magnitude of the 869 Jogan tsunami using sedimentary deposits: prediction and consequence of the 2011 Tohoku-oki tsunami, *Sediment. Geol.,* **282,** 14–26.

Symithe, S., Calais, E., de Chabalier, J.B., Robertson, R. & Higgins, M., 2015. Current block motions and strain accumulation on active faults in the Caribbean, *J. geophys. Res.,* **120**(5), 3748–3774.

Synolakis, C.E., Bardet, J.-P., Borrero, J.C., Davies, H.L., Okal, E.A., Silver, E.A., Sweet, S. & Tappin, D.R., 2002. The slump origin of the 1998 Papua New Guinea tsunami, *Proc. Roy. Soc. Lond., A,* **458,** 763–789.

Tabrez Ali, S., Fred, A.M., Calais, E., Manaker, D.M. & McCann, W.R., 2008. Coulomb stress evolution in Northeastern Caribbean over the past 250 years due to coseismic, postseismic and interseismic deformation, *Geophys. J. Int.,* **174**(3), 904–918.

Tadepalli, S. & Synolakis, C.E., 1996. Model for the leading waves of tsunamis, *Phys. Rev. Lett.,* **77**(10), 2141–2144.

Tanner, J.G. & Shepherd, J.B., 1997. Seismic hazard in Latin America and the Caribbean. Instituto Panamericano de Geografía e Historia, and Intl. Development Res. Centre, Ottawa, 12 pp.

ten Brink, U.S., Bakun, W.H. & Flores, C.H., 2011. Historical perspective on seismic hazard to Hispaniola and the northeast Caribbean region, *J. geophys. Res.: Solid Earth,* **116**(B12), 1978–2012.

Verbeek, R.D.M., 1900. Kort verslag over de aard- en zeebeving op Ceram, den 30sten September 1899, *Natuurkundig Tijdschrift voor Nederlandsch-Indië,* **60,** 219–228.

von Hillebrandt-Andrade, C., Aliaga, B. & Edwards, S., 2013. Educating and Preparing for Tsunamis in the Caribbean, *EOS, Trans. Am. Geophys. Un.,* **94**(53), abstract #ED43D-0785.